



## Molecular cloning and knockdown of *galactocerebrosidase* in zebrafish: New insights into the pathogenesis of Krabbe's disease

Daniela Zizioli <sup>a,1</sup>, Michela Guarienti <sup>a,1</sup>, Chiara Tobia <sup>b</sup>, Giuseppina Gariano <sup>b</sup>, Giuseppe Borsani <sup>c</sup>, Roberto Bresciani <sup>a</sup>, Roberto Ronca <sup>b</sup>, Edoardo Giacomuzzi <sup>c</sup>, Augusto Preti <sup>a</sup>, Germano Gaudenzi <sup>d</sup>, Mirella Belleri <sup>b</sup>, Emanuela Di Salle <sup>b</sup>, Gemma Fabrias <sup>e</sup>, Josefina Casas <sup>e</sup>, Domenico Ribatti <sup>f,g</sup>, Eugenio Monti <sup>a</sup>, Marco Presta <sup>b,\*</sup>

<sup>a</sup> Unit of Biotechnology, Department of Molecular and Translational Medicine, University of Brescia, Brescia, Italy

<sup>b</sup> Unit of Oncology and Experimental Immunology, Department of Molecular and Translational Medicine, University of Brescia, Brescia, Italy

<sup>c</sup> Unit of Biology and Genetics, Department of Molecular and Translational Medicine, University of Brescia, Brescia, Italy

<sup>d</sup> Department of Biology, University of Milan, Milan, Italy

<sup>e</sup> Research Unit on Bioactive Molecules (RUBAM), Department of Biomedical Chemistry, Institute for Advanced Chemistry of Catalonia (IQAC), Spanish Council for Scientific Research (CSIC), Barcelona, Spain

<sup>f</sup> Department of Basic Biomedical Sciences, Unit of Human Anatomy and Histology, University of Bari, Bari, Italy

<sup>g</sup> National Cancer Institute, Giovanni Paolo II, Bari, Italy

### ARTICLE INFO

#### Article history:

Received 2 September 2013

Received in revised form 17 December 2013

Accepted 15 January 2014

Available online 24 January 2014

#### Keywords:

Galactosylceramidase  
Embryonic development  
Krabbe disease  
Sphingolipid  
Zebrafish

### ABSTRACT

The lysosomal hydrolase galactocerebrosidase (GALC) catalyzes the removal of galactose from galactosylceramide and from other sphingolipids. GALC deficiency is responsible for globoid cell leukodystrophy (GLD), or Krabbe's disease, an early lethal inherited neurodegenerative disorder characterized by the accumulation of the neurotoxic metabolite psychosine in the central nervous system (CNS). The poor outcome of current clinical treatments calls for novel model systems to investigate the biological impact of GALC down-regulation and for the search of novel therapeutic strategies in GLD. Zebrafish (*Danio rerio*) represents an attractive vertebrate model for human diseases. Here, lysosomal GALC activity was demonstrated in the brain of zebrafish adults and embryos. Accordingly, we identified two *GALC* co-orthologs (named *galca* and *galcb*) dynamically co-expressed in CNS during zebrafish development. Both genes encode for lysosomal enzymes endowed with GALC activity. Single down-regulation of *galca* or *galcb* by specific antisense morpholino oligonucleotides results in a partial decrease of GALC activity in zebrafish embryos that was abrogated in double *galca/galcb* morphants. However, no psychosine accumulation was observed in *galca/galcb* double morphants. Nevertheless, double *galca/galcb* knockdown caused reduction and partial disorganization of the expression of the early neuronal marker *neuroD* and an increase of apoptotic events during CNS development. These observations provide new insights into the pathogenesis of GLD, indicating that GALC loss-of-function may have pathological consequences in developing CNS independent of psychosine accumulation. Also, they underscore the potentiality of the zebrafish system in studying the pathogenesis of lysosomal neurodegenerative diseases, including GLD.

© 2014 Elsevier B.V. All rights reserved.

### 1. Introduction

Lysosomal storage disorders represent one of the most frequent classes of human genetic diseases. Galactocerebrosidase (GALC; EC 3.2.1.46) [1] is a lysosomal acid hydrolase that catalyzes the removal of galactose from galactosylceramide (GalCer), a major component of myelin, and from other terminal  $\beta$ -galactose-containing sphingolipids,

including galactosyl-sphingosine (psychosine). Genetic GALC deficiency causes globoid cell leukodystrophy (GLD), or Krabbe's disease (OMIM #245200), an autosomal recessive sphingolipidosis characterized by degeneration of oligodendroglia and progressive demyelination. The pathogenesis of the disease has been proposed to arise from the accumulation of the neurotoxic GALC metabolite psychosine detectable at high levels in the central nervous system (CNS) of GLD patients [2–4].

Clinically, GLD manifests in early infancy and results in a severe neurological dysfunction that often leads to death by 2 years of age [5–7]. At present, the only clinical treatment for GLD is bone marrow or umbilical cord blood cell transplantation for late-onset and presymptomatic patients [7,8]. Thus, novel model systems may provide an invaluable tool for investigating the molecular mechanisms underlying GLD in the search for effective therapeutic interventions. The *twitcher* mouse is an

**Abbreviations:** GALC, galactocerebrosidase; GLD, globoid cell leukodystrophy; CNS, central nervous system; hpf, hours post fertilization; MO, morpholino oligonucleotide; GalCer, galactosylceramide; psychosine, galactosylsphingosine

\* Corresponding author at: Department of Molecular and Translational Medicine, Viale Europa 11, 25123 Brescia, Italy. Tel.: +39 30 3717311; fax: +39 30 3717747.

E-mail address: [presta@med.unibs.it](mailto:presta@med.unibs.it) (M. Presta).

<sup>1</sup> D.Z. and M.G. contributed equally to this work.

authentic murine model of GLD widely used to understand the molecular and biochemical bases of the disease and as a model system for novel therapeutic approaches [9–12]. Nevertheless, such studies in mice can be relatively slow, laborious and expensive to perform. Also, the intra-uterine gestation makes it difficult to follow possible alterations in developmental processes consequent to the lack of GALC activity.

When compared to other vertebrate models, zebrafish (*Danio rerio*) offers several features that make this freshwater fish an attractive vertebrate system to investigate the mechanisms of human diseases alternative to mouse [13,14]. The nervous system in zebrafish is well characterized and considered suitable for comparison to humans [15,16], making zebrafish a possible alternative organism to investigate human neurodegenerative and lysosomal storage diseases [16–19]. Also, a comprehensive collection of reverse genetics tools have been developed for studying gene function in this useful organism. Microinjection of antisense morpholino oligonucleotides (MOs) into one cell embryos can be used to assess the effect of transient gene down-regulation on early zebrafish development [20,21]. Moreover, engineered endonucleases, including ZFNs (zinc finger nucleases), TALENs (transcription activator-like effector nucleases) and clustered, regularly interspaced, short palindromic repeats (CRISPR)–CRISPR-associated (Cas) systems, have been shown to provide new and efficient strategies to achieve directly site-specific genome modification in zebrafish [22,23].

In the present study, lysosomal GALC activity was demonstrated in the brain of zebrafish adults and embryos. Accordingly, *in silico* analysis identified two zebrafish gene orthologs to mammalian GALC (named *galca* and *galcb*). Both genes encode for lysosomal enzymes active at acidic pH when transduced in HEK cells. Whole-mount *in situ* hybridization (WISH) experiments demonstrated that *galca* and *galcb* are expressed in CNS during zebrafish development. Following specific MO injection, *galca/galcb* double morphants were characterized by the complete down-regulation of GALC activity in zebrafish embryos. However, no psychosine accumulation was observed in *galca/galcb* double morphants that did not show major phenotypic developmental alterations. Nevertheless, double *galca/galcb* knockdown caused the reduction and partial disorganization in the expression of the neuronal marker *neuroD* [24] and an increase of apoptotic events in developing zebrafish CNS, indicating that GALC loss-of-function may have pathological consequences in developing CNS independent of psychosine accumulation. These observations, together with the lack of lethal embryonic defects in zebrafish morphants, set the bases for future studies aimed at investigating the effect of stable *galca/galcb* gene knock-out in zebrafish for the study of the pathogenesis of GLD and for the search of efficacious therapeutic strategies.

## 2. Materials and methods

### 2.1. Zebrafish maintenance and collection

All embryos were handled according to relevant national and international guidelines. Current Italian rules do not require approval for research on zebrafish embryos. The wild type zebrafish AB strain was maintained at 28 °C on a 14 h light/10 h dark cycle under standard laboratory conditions as described in the Zebrafish Book [25]. Immediately after spawning, the fertilized eggs were harvested, washed and placed in 10 cm Ø Petri dishes in fish water. The developing embryos were incubated at 28 °C. Embryos at different stages were maintained in 0.003% 1-phenyl-2-thiourea (Sigma) to prevent pigmentation. Embryos were fixed in 4% paraformaldehyde in PBS overnight at 4 °C, rinsed twice in 1% Tween-20 in PBS, dehydrated in methanol and stored at –20 °C until processing [26].

### 2.2. Bioinformatics analysis and protein modeling

Nucleotide and amino acid sequences were compared to the non-redundant sequence databases present at the NCBI (National Center

for Biotechnology Information GenBank Database, <http://blast.ncbi.nlm.nih.gov>) using the BLAST algorithm [27]. Sequence similarity searches against the Zebrafish Jul. 2010 (Zv9/danRer7) genome assembly were performed using Blat at the UCSC Genome Browser (<http://genome.ucsc.edu/>). The multiple sequence alignment was generated using ClustalW [28] and phylogenetic analysis was performed on the Phylogeny.fr web service. Comparative genomics analysis of Galc sequences in teleosts was performed using the Ensemble db (<http://www.ensembl.org>). Synteny analysis was carried out using the Genomicus genome browser (<http://www.dyogen.ens.fr/genomicus-72.01>) [29].

Structural models of *D. rerio* Galca and Galcb proteins were obtained by similarity modeling using I-Tasser (PMID: 20360767) and the known crystal structure of the mouse GALC protein as template (pdb entry: 3zr6). The predicted models with the lowest C-score were selected as the putative protein structures. Pdb models of Galca and Galcb were then superimposed on the murine protein structure using PyMOL (The PyMOL Molecular Graphics System, Version 1.5.0.1 Schrödinger, LLC).

### 2.3. Cloning, sequencing and expression of zebrafish *galca* and *galcb* genes

Total RNA was isolated from zebrafish embryos at 4 h post fertilization (hpf). The full coding regions of *galca* and *galcb* genes were amplified by RT-PCR using the following specific primers:

*galca*: forward, 5'-cagacttcagccgagcttcattg-3'; reverse, 5'-gtcagaatcacccctgcaatcac-3';

*galcb*: forward, 5'-ggaacgcacgggtagaataatgtac-3'; reverse, 5'-gtatgggtgttattctgctc-3'.

The RT-PCR products were electrophoresed on 1% agarose gel in 1 × TAE buffer, ethidium bromide stained and then cloned directly into the pCR®2.1-TOPO vector (Invitrogen). After sequencing verification, the *galca* cDNA was excised with *BstXI* and the *galcb* cDNA was digested with *XbaI* and *BamHI*; the inserts were then subcloned into the pcDNA 3.1 expression vector. The constructs were stably transfected in HEK293T cells using lipofectamine according to standard protocols.

### 2.4. GALC activity assays

Routinely, GALC activity was measured as described [30]. Briefly, 10 µg of protein extract (50 µl) were mixed with 100 µl of 1.5 mM 4-methylumbelliferyl-β-D-galactoside substrate (Sigma) resuspended in 0.1/0.2 M citrate/phosphate buffer, pH 4.0, in the presence of 20 µM AgNO<sub>3</sub> to inhibit β-galactosidase activity. Reactions were incubated for 30 min at 37 °C, stopped with 0.2 M glycine/NaOH, pH 10.6, and fluorescence of released 4-methylumbelliferone was measured (λ<sub>ex</sub> 360 nm, λ<sub>em</sub> 446 nm). When indicated, GALC-mediated lysis of the synthetic fluorescent GALC substrate LRh-6-GalCer (*N*-lissamine rhodaminyl-6-aminohexanoylgalactosyl ceramide) following its incubation with 40 µg of tissue extract was quantified by thin-layer chromatography as described [31]. In some experiments, the assays were performed in the presence of a 10-fold more excess of psychosine or *N*-acetyl-D-sphingosine (Sigma). In that case, the concentration of the 4-methylumbelliferyl-β-D-galactoside substrate was equal to 0.2 mM.

### 2.5. Western blot analysis

Total cell proteins were isolated using the RIPA lysis buffer (50 mM Tris-HCl, 50 mM NaCl, 1% Triton X-100, 1 mM EDTA) containing protease inhibitors, subjected to 3 rounds of sonication, and incubated for 45 min on ice. Protein content was measured using the Bradford Protein Assay Kit (BioRad) with bovine serum albumin as the reference standard. Protein samples were subjected to SDS/PAGE [10% (w/v) polyacrylamide

gel] and subsequently transferred by electroblotting onto an Immobilon-P blotting membrane (Amersham Biosciences). The membranes were incubated for 30 min in PBST [PBS containing 0.05% (v/v) Tween 20] and 5% (w/v) non-fat dried skimmed milk powder (blocking buffer) and subsequently incubated with a rabbit polyclonal anti-human GALC antibody (Proteintech, catalog no. 11991-1-AP). After a final washing in PBST and incubation with horseradish-peroxidase-conjugated anti-rabbit antibody (ThermoScientific), immunoreactive proteins were visualized using the SuperSignal West Pico chemiluminescence substrate detection kit (Pierce).

## 2.6. Subcellular fractionation on Percoll gradients

HEK293T transfected cells were washed with PBS/0.25 M sucrose at 4 °C, scraped in 0.25 M sucrose/2.5 mM Tris buffer, pH 7.4 (buffer A) and centrifuged at 800 × g for 10 min. Cells were resuspended in 1 ml buffer A, homogenized with Dounce homogenizer (40 strokes) and centrifuged at 1200 × g for 10 min. The postnuclear supernatant was loaded on 10 ml Percoll solution (20% Percoll, 0.25 M sucrose, 5 mM Tris buffer, pH 7.2) and centrifuged for 30 min at 35,000 × g in the vertical rotor VTi 65.1 (Beckman Instruments) [32]. In some experiments, brain extracts from zebrafish adults (200 mg of protein) were prepared in buffer A and loaded on the top of the Percoll gradient. Then, GALC activity assay was performed for each fraction and β-hexosaminidase activity was used as a lysosomal marker.

## 2.7. Quantitative RT-PCR analysis

RNA samples were extracted from zebrafish embryos at different developmental stages following TRIzol® reagent protocol (Invitrogen) and treated with RQ1 RNase-Free DNase (Promega). Two micrograms of total RNA was retrotranscribed with MMLV reverse transcriptase (Invitrogen), using random hexamers in a final volume of 20 μl. Quantitative RT-PCR was performed with a Biorad iCycler iQ™ Real-time PCR Detection System using a iQ™ SYBR Green Supermix (BioRad) according to manufacturer's instructions using the following specific primers at 400 mM final concentration:

*galca*: forward, 5'-GCGATGGCTCAAACCCACAG-3'; reverse, 5'-AAGT AAGGCCATTGGGTTTC-3';  
*galcb*: forward, 5'-TGGTGGGCGTTACTTGTTC-3'; reverse, 5'-ATGTGT GAGGGCTCAGTTCC-3'.

Triplicate data were averaged and normalized to an averaged 18S rRNA endogenous control [33]. Data were analyzed using REST [34].

## 2.8. Immunofluorescence analysis

Seven micrometer thick OCT-embedded frozen serial coronal sections from the brain of zebrafish adults were fixed for 2 min in cooled acetone, air dried, and washed three times with Tris-buffered saline. After blocking with 1% BSA in PBS plus 0.1% Triton X-100, sections were incubated overnight at 4 °C with rabbit polyclonal anti-GALC antibody (1:100, Proteintech) or with rabbit polyclonal anti-GFAP antibody (1:100, Dako Glostrup), followed by 1 h incubation at room temperature with Alexa Fluor 488 anti-rabbit IgG antibody (1:250, Invitrogen). For double-immunolabeling the sections were incubated overnight at 4 °C with anti-GALC antibody (1:100) and a mouse monoclonal anti-GAD67 antibody (1:100, Millipore, clone 1G10.2), followed by 1 h incubation with Alexa Fluor 488 anti-rabbit IgG antibody (1:250) plus Alexa Fluor 594 anti-mouse IgG antibody (1:250). Nuclei were counterstained with 4,6-diamidino-2-phenylindole (DAPI, Sigma). Images were acquired using an Axiovert 200 microscope (Zeiss) equipped with ApoTome optical sectioning device (Zeiss).

## 2.9. Whole-mount *in situ* hybridization

Antisense and sense riboprobes were prepared by *in vitro* transcribed linearized cDNA clones with T7 and SP6 polymerase using Digoxigenin Labeling Mix (Roche). The probes specific for *galca* and *galcb* genes were selected in order to avoid cross hybridization between the two genes using the following specific primers:

*galca*: forward, 5'-gcactttgacgtctctcc-3'; reverse, 5'-agataaagtctcctagcagc-3';  
*galcb*: forward, 5'-ggtgggagttacgttgact-3'; reverse, 5'-gagcactgcattctccaca-3'.

For the *galca* probe a PCR fragment of 840 bp and for *galcb* probe a PCR fragment of 863 bp were subcloned in the pCR®2.1-TOPO vector (Invitrogen). The anti-sense probes for *galca* and *galcb* containing the ATG were synthesized with T7 polymerase by transcribing the *Sall*-linearized *galcap*CR2.1-TOPO and the *HindIII*-linearized *galcbp*CR2.1-TOPO vectors, respectively.

Whole-mount *in situ* hybridization (WISH) was carried out as described [35]. After fixation, 0.003% 1-phenyl-2-thiourea-treated embryos at different developmental stages were permeabilized with Proteinase K (10 μg/ml, Sigma) and hybridized overnight at 68 °C in formamide buffer with Digoxigenin-labeled RNA antisense or sense probes. After several washes at high stringent temperature, NBT/BCIP (Roche) staining was performed according to manufacturer's instructions. Embryos were mounted in agarose-coated dishes and images were taken with a Leica MZ16F stereomicroscope equipped with DFC 480 digital camera and LAS Leica Imaging software (Leica, Wetzlar, Germany).

## 2.10. Morpholino knockdown

Specific MOs (Gene Tools, Philomath, OR) were designed targeting the exon 3 of zebrafish *galca* and *galcb* genes:

*galca*: MO 5'-TACITTTGCTTACCTGTGGTTT-3';  
*galcb*: MO 5'-GCAGAGTTTACCTGTAGTCTG-3'.

MOs, diluted in Danieau buffer, were injected at the 1–2-cell stage. Increasing doses of each MO were tested for phenotypic effects; as control for nonspecific effects, experiments were performed in parallel with a standard control MO (std MO) (Gene Tools, Philomath, OR) with no targets in zebrafish embryos. For double gene knockdown experiments, increasing doses of the two MOs were co-injected and assessed for phenotypic effects: routinely, embryos were co-injected with 0.4 pmol/embryo of *galca*-MO and/or 1.4 pmol/embryo of *galcb*-MO.

To confirm the targeting efficacy of the two MOs, alternative splicing pattern analysis was performed on zebrafish embryos using the following RT-PCR primers:

*galca*: forward, 5-cagacttcagccgactgtcatt-3'; reverse, 5'-aagccaccac tcgatccac-3';  
*galcb*: forward, 5'-ttgatggcattggtggatta-3'; reverse, 5'-ctctcttggtccacat-3'.

## 2.11. Quantitative acridine orange apoptosis test

The apoptosis test was performed on 24 hpf embryos as described [36]. Briefly, dechorionated embryos were stained with 1.0 μg/ml acridine orange (Sigma). Then, embryos were washed with fish water, anesthetized in tricaine (ethyl 3-aminobenzoate methanesulfonate salt, Sigma) and distributed into 96-well plates, five embryos per well. After lysis in 100% ethanol, fluorescence was measured at λ<sub>exc</sub> 490 nm/λ<sub>em</sub> 525 nm with a microplate reader (Tecan Infinite M200). The apoptosis data

were confirmed by epifluorescent microscopy analysis of the embryos (ApoTome, Zeiss).

## 2.12. Psychosine analysis

Quantification of psychosine (galactosyl-sphingosine plus glucosyl-sphingosine) was conducted on pools of 100 zebrafish embryos. The brain of wild type and *twitcher* mice were used as controls. Lyophilized tissues were homogenized in 120  $\mu$ l of PBS and lipids were extracted as reported [37]. Samples were analyzed in a Ultra-Performance Liquid Chromatography apparatus coupled to an orthogonal acceleration time-of-flight mass spectrometer with an electrospray ionization interface (LCT Premier, Waters) using gradient program and instrumental parameters previously described [37]. Data were acquired under positive (ESI+) ionization mode over a mass range of  $m/z$  50–1800 in W-mode. A scan time of 0.15 s and interscan delay of 0.01 s were used at a nominal instrument resolution of 11.500 (FWHM). Leucine enkephalin was used

as the lock spray calibrant. The detection limit of the method was equal to 25 pmol of psychosine/g dry tissue.

## 3. Results

### 3.1. Identification of GALC activity in zebrafish

In order to assess the presence of an enzymatic GALC activity in zebrafish, a set of preliminary experiments were performed on brain tissue harvested from 4 month-old zebrafish adults. As shown in Fig. 1A, B, a significant GALC activity was detectable in the zebrafish brain tissue extract following its incubation with the fluorescent GALC substrate LRh-6-GalCer [31] or with the 4-methylumbelliferyl- $\beta$ -D-galactoside substrate, the latter incubation being performed in the presence of 20  $\mu$ M AgNO<sub>3</sub> to inhibit  $\beta$ -galactosidase activity [30]. In both assays, the extracts from murine wild-type and *twitcher* brains were used as positive and negative controls, respectively. Also, in both assays degradation of the substrate was competed by a 10-fold molar excess of the GALC substrate

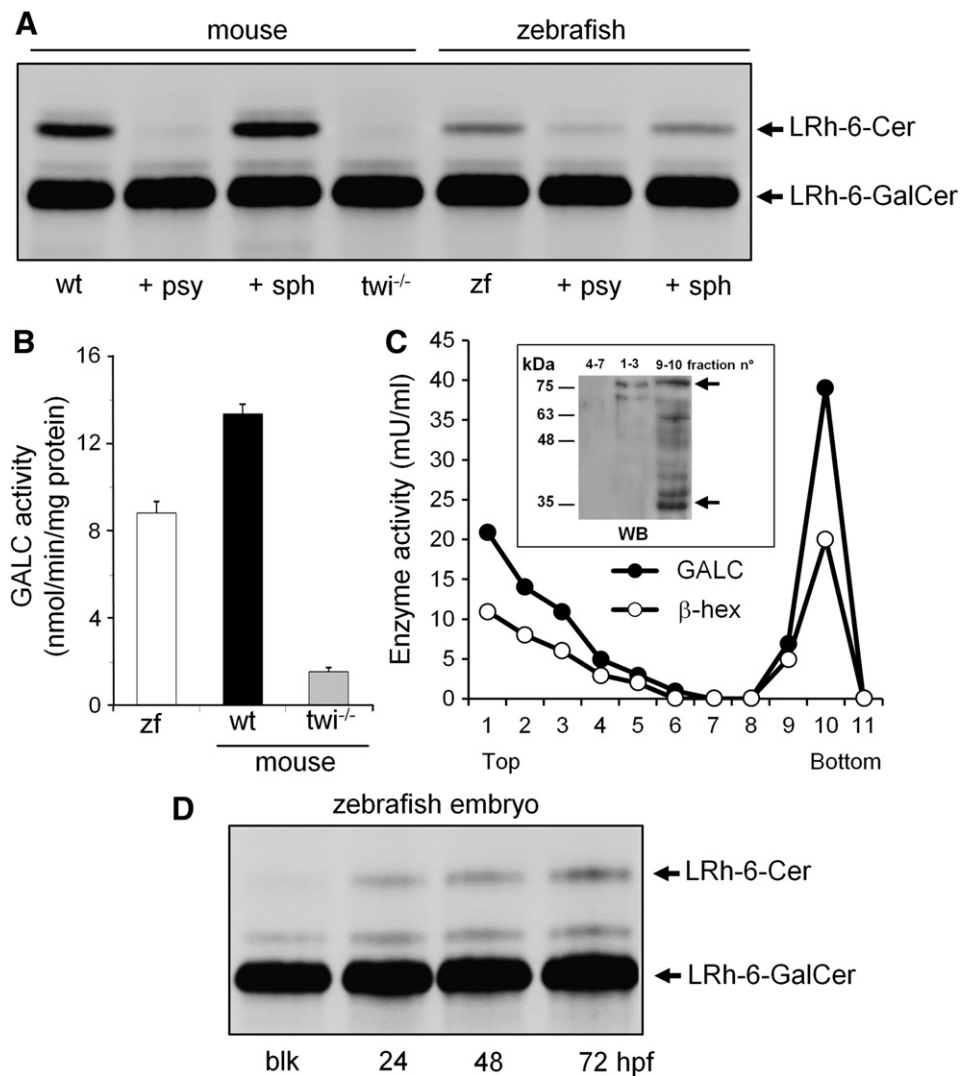


**Fig. 1.** GALC activity in zebrafish. **A**, Brain extracts (40  $\mu$ g of protein) from 4 month-old zebrafish adults (zf) were evaluated for GALC activity using the GALC substrate LRh-6-GalCer in the absence or in the presence of a 10-fold molar excess of psychosine (psy) or *N*-acetyl-*D*-sphingosine (sph). In this assay, LRh-6-GalCer is converted to LRh-6-Cer and the two fluorescent compounds are separated by thin layer chromatography and visualized under an ultraviolet lamp. Brain extracts from wild-type (wt) and GALC-deficient *twitcher* (*twi*<sup>-/-</sup>) mice were used as positive and negative controls, respectively. **B**, Brain extracts (10  $\mu$ g of protein) from zebrafish adults (zf) and from wt and *twi*<sup>-/-</sup> mice were assessed for GALC activity using the 4-methylumbelliferyl- $\beta$ -D-galactoside substrate (1.5 mM) in the presence of 20  $\mu$ M AgNO<sub>3</sub> to inhibit  $\beta$ -galactosidase activity [30]. **C**, Subcellular fractionation on Percoll density gradient of the brain extract of zebrafish adults. GALC activity co-sediments with the lysosomal  $\beta$ -hexosaminidase enzyme marker ( $\beta$ -hex). Values are representative of 3 independent experiments. *Inset*, Western blot (WB) analysis of the indicated pooled fractions of the gradient (5  $\mu$ g of protein) shows the presence of an immunoreactive 30 kDa lysosomal-processed enzyme fragment and of the uncleaved 80 kDa protein (arrows) in the dense lysosome-containing fractions. **D**, Extracts (40  $\mu$ g of protein) from zebrafish embryos at different stages of development were evaluated for GALC activity using the GALC substrate LRh-6-GalCer. blk, blank reaction in the absence of embryo extract.

psychosine but not by control *N*-acetyl-D-sphingosine (Fig. 1A and Supplementary Fig. 1A).

In keeping with the enzymatic activity assays, immunohistochemical analysis of the brain of zebrafish adults showed the presence of a punctate distribution of GALC immunoreactivity in both glial and neuronal cells (Supplementary Fig. 2). On this basis, to confirm the lysosomal localization of GALC activity in zebrafish CNS, subcellular fractionation of brain tissue extract was performed using Percoll density gradient analysis [32]. Similar to the lysosomal marker  $\beta$ -hexosaminidase, more than 50% of the total GALC activity present in the brain of zebrafish adults was recovered in the dense lysosome-containing fractions of the gradient (fractions 9–10) (Fig. 1C). Accordingly, GALC-immunoreactive bands corresponding the 30 kDa lysosomal-processed enzyme fragment and the uncleaved 80 kDa protein ([38] and references therein) were detectable by Western blotting in the dense lysosome-containing fractions of the gradient (Fig. 1C, inset).

To assess the presence of GALC activity also in zebrafish embryos, the head region was dissected from embryos at 24, 48 and 72 h post fertilization (hpf) and tissue extracts were incubated with the fluorescent GALC substrate LRh-6-GalCer. As shown in Fig. 1D, a significant GALC activity was detectable at all the time point investigated.

Together, the data demonstrate the presence of a *bona-fide* GALC activity in zebrafish adults and embryos.

### 3.2. Cloning and characterization of GALC gene orthologs in zebrafish

In order to identify the GALC gene ortholog(s) in zebrafish, the amino acid sequence of human GALC protein was used as query in a Blat search performed against the UCSC Genome Browser on Zebrafish Jul. 2010 (Zv9/danRer7) assembly. Two gene sequences encoding polypeptides homologous to human GALC were identified on zebrafish chromosomes 20 and 17, named *galca* (acc. no. NM\_001005921) and *galcb* (acc. no. NM\_213111), respectively. Further bioinformatic analysis on nucleotide and protein sequences present in the NCBI databases, performed using the BLAST algorithm, failed to identify additional *galc* genes in zebrafish.

Both *galca* and *galcb* genes are transcribed as demonstrated by the presence of 14 and 47 ESTs in the corresponding UniGene clusters, respectively. Also, RNA-Seq data from pooled zebrafish tissues, provided by Wellcome Trust Sanger Institute, suggest that *galcb* is globally more expressed than its paralog (data not shown) (PMID: 22798491).

The *galca* and *galcb* coding sequences were cloned by RT-PCR from total RNA isolated from zebrafish embryos at 4 h post fertilization (hpf). DNA sequencing confirmed that *galca* and *galcb* cDNAs encode for predicted polypeptides of 660 (acc. no. NP\_001005921) and 664 (acc. no. NP\_998276) amino acids, respectively, with 66% identity and 79% similarity. A comparison of Galca and Galcb polypeptides with mammalian GALC proteins revealed a high degree of amino acid sequence identity (61%), with a large number of residue blocks highly conserved along the primary structure (Supplementary Fig. 3). According to the Carbohydrate-Active enZYmes Database (CAZY) [39], zebrafish Galca and Galcb polypeptides belong to the glycoside hydrolase family 59, a class of galactosylcerebrosidase enzymes that includes also human and mouse GALC.

Zebrafish *galca* and *galcb* genes share the same 17 exons/16 introns structure of human and murine genes. Regions of conserved synteny are observed between human chromosome 14, harboring the GALC gene, and *D. rerio* chromosomes 17 and 20 (Supplementary Fig. 4A). Also, duplicated genes other than *galc* are present on zebrafish chromosomes 17 and 20, suggesting that this region represents one of the remnants of an ancient genome duplication event that occurred shortly before the teleost radiation [40]. Interestingly, the analysis of genomic sequences of other teleosts revealed that Fugu (*Takifugu rubripes*), Medaka (*Oryzias latipes*), Stickleback (*Gasterosteus aculeatus*) and Tetraodon (*Tetraodon nigroviridis*) all possess a single *galc* gene. A phylogenetic tree of some vertebrate GALC proteins is shown in Supplementary Fig. 4B.

Given the high level of sequence identity between zebrafish Galc proteins with the mouse orthologous polypeptide, we performed a homology modeling analysis using the crystal structure of the mouse GALC protein as template [38]. We obtained two structural models for *D. rerio* Galca and Galcb, with a C-score of 0.91 and 0.30 and a calculated RMSD of  $0.84 \pm 0.08$  and  $0.75 \pm 0.10$ , respectively. As expected from the high protein sequence similarity, the models fit well on the mouse template when superimposed with PyMOL. Both Galca and Galcb predicted structures show the presence of the three domains described for mouse GALC [38]: a TIM barrel domain responsible for the enzymatic activity, a lectin domain involved in substrate recognition and a  $\beta$ -sandwich domain (Fig. 2A). Analysis of the protein structures reveals slightly differences in this latter region that appears to be formed by 6 rather than 7 well-defined  $\beta$ -sheets in Galcb. The position of the four catalytic residues (T109, E198, E274, R396) and the organization of the active site are fully conserved (Fig. 2B) as well as the position of the N-glycosylation site N379 and of the cysteine residues C287 and C394 involved in an intramolecular stabilizing disulphide bond [38]. Also, amino acids, W307 and T109, that confer substrate specificity for galactose- rather than glucose-containing glycolipids, are in topologically conserved positions. Most of the residues that are not conserved between mammalian and zebrafish GALC enzymes are exposed on the surface of the predicted *D. rerio* structures (data not shown).

In conclusion, our data indicate that *galca* and *galcb* are two zebrafish co-orthologs for the mammalian GALC gene and encode for proteins with high similarity to their mammalian counterpart.

### 3.3. Biochemical characterization of zebrafish Galca and Galcb enzymes

In order to characterize the biochemical features of *galca* and *galcb* encoded proteins, human HEK293T cells were stably transfected with the corresponding cDNAs. Western blot analysis with a rabbit polyclonal anti-GALC antibody confirms the increase in the levels of the 30 kDa immunoreactive lysosomal-processed enzyme fragment ([38] and references therein) in the cell extracts of both *galca*- and *galcb*-transfected cells when compared to mock-transfected cells (Fig. 3A), whereas the uncleaved form of the enzyme was below the limits of detection of the method in all the transfectants. Accordingly, *galca* and *galcb* overexpression leads to a 4–5 fold increase in GALC activity in transfected cells when compared to mock transfectants (Fig. 3B). For both transfectants this increase of activity was inhibited by a 10-fold molar excess of the GALC substrate psychosine but not by control *N*-acetyl-D-sphingosine (Supplementary Fig. 1B). Finally, the GALC activity expressed by *galca*- and *galcb*-transfected cells showed a pH optimum equal to 4.0 (Fig. 3C) and Percoll density gradient analysis confirmed that most of the activity of both enzymes was recovered in the dense  $\beta$ -hexosaminidase-positive lysosomal fractions of the gradient (Fig. 3D).

Mannose-6-phosphate (M6P) inhibits the M6P receptor-mediated cellular uptake of newly-synthesized lysosomal enzymes, leading to their miss-sorting into the extracellular space [41]. Accordingly, in keeping with the lysosomal nature of Galca and Galcb proteins, incubation of HEK293T transfectants with 5 mM M6P leads to lysosomal enzyme miss-sorting with a significant increase in both GALC and  $\beta$ -hexosaminidase activities present in their conditioned medium when compared to untreated transfectants (Fig. 3E). Overall, the results demonstrate that zebrafish *galca* and *galcb* genes encode for lysosomal enzymes endowed with GALC activity.

### 3.4. Temporal and spatial pattern expression of galca and galcb during zebrafish development

The expression of *galca* and *galcb* genes was investigated during embryonic and early larvae development in zebrafish by quantitative RT-PCR and WISH analysis. We took care to design specific sets of RT-PCR primers and WISH probes in order to avoid cross-reactivity between the two *galc* transcripts. As shown in Fig. 4A, B, *galca* and *galcb*

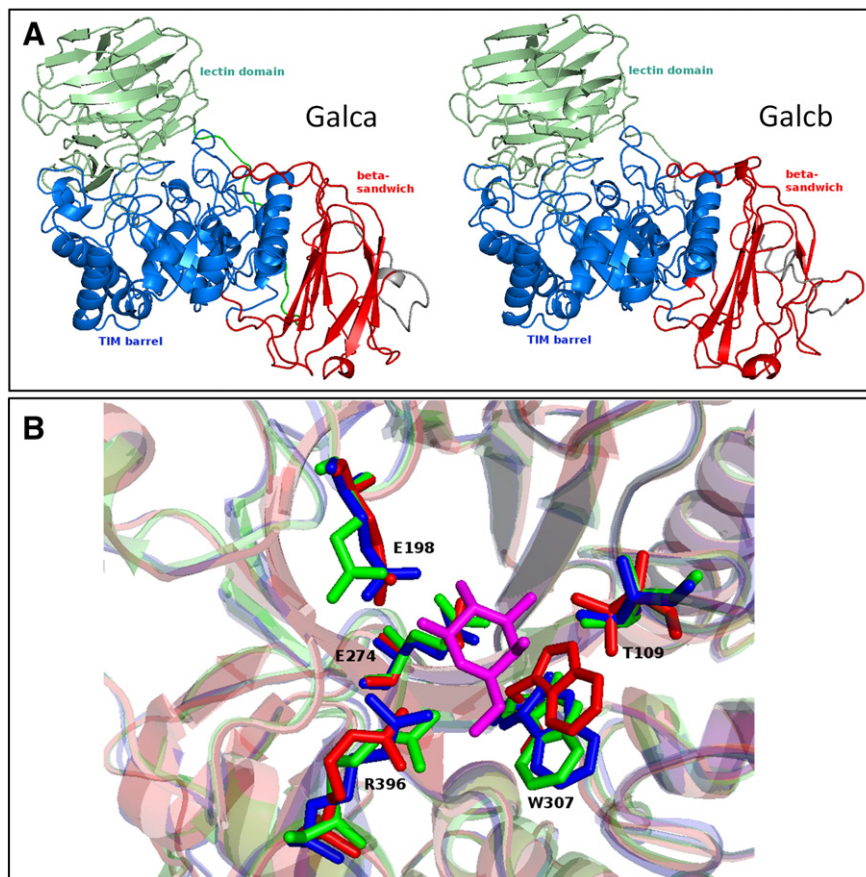


**Fig. 2.** Structural models of *Danio rerio* Galca and Galcb proteins obtained by similarity modeling. A, Ribbon diagram of zebrafish Galca (left) and Galcb (right) colored by domain:  $\beta$ -sandwich (red), TIM barrel (blue), linker (orange), and lectin domain (green). B, Structure of the active site of GALC. The predicted structures of *D. rerio* Galca, in green, and Galcb, in blue, were superimposed to the known crystal structure of mouse Galc (pdb: 3zr6), in red. The organization of the active site and the position of catalytic residues T109, E198, E274 and R396 are conserved between mouse and *D. rerio* co-orthologs. The substrate galactose, placed in the catalytic crevice, is shown in magenta. Substrate specificity for galactose- rather than glucose-containing glycolipids is conferred by amino acids W307 and T109. Numbering of residues is relative to the mouse Galc RefSeq protein (NP\_032105) and differs of 16 amino acids from the sequence of mouse GALC structure [38].

mRNAs were already detectable by quantitative RT-PCR at 8-cell stage, pointing to a maternal origin of both transcripts. Then, the total levels of *galca* and *galcb* mRNAs decreased, to remain constant throughout development from the 6-somite stage to 48 hpf.

WISH analysis confirmed the expression of both *galca* and *galcb* in zebrafish embryos at 1.25 hpf and 5 hpf (Fig. 4C, D). In the segmentation period the expression of *galca* and *galcb* persists; labeling is detectable in the rostral part of the embryos in developing CNS whereas the signal is progressively excluded from the notochord. At 24 hpf, the expression of both genes is observed in defined areas of the brain, including mid-brain, midbrain–hindbrain boundary, hindbrain and cerebellum. At 48 hpf, *galca* and *galcb* expression is maintained mainly in midbrain–hindbrain boundary and hindbrain. In all WISH experiments, no specific signal was observed when embryos were hybridized with a sense probe (data not shown). Together with the GALC activity data (see Fig. 1D), these results indicate that *galca* and *galcb* are co-expressed from early stages of CNS development in zebrafish.

### 3.5. *galca/galcb* knockdown in zebrafish embryos

To investigate the effect of *galca* and *galcb* down-regulation at the early stages of zebrafish development, we performed loss-of-function studies using the MO knockdown approach. This results in a transient silencing of the targeted gene that lasts for the first few days of development [20,21]. To this purpose, specific MOs were designed to induce skipping of exon 3 of the immature *galca* or *galcb* mRNAs. In both cases the MOs were predicted to cause the formation of enzymatically inactive proteins. RT-PCR analysis of single and double *galca* and *galcb*

morphants performed at 48 hpf confirmed the targeting efficacy of the two MOs with *galca* MO causing both partial and total skipping of exon 3 and *galcb* MO causing the complete skipping of exon 3 (data not shown and Fig. 5A for double *galca/galcb* morphants). Also, the total GALC activity present in the protein extract of 24 hpf and 48 hpf embryos was significantly reduced but not abolished by single *galca* or *galcb* knockdown (Fig. 5B). On this basis, the effect of the co-injection of increasing doses of both MOs was tested for phenotypic effects and optimum concentrations of 0.4 pmol/embryo and 1.4 pmol/embryo were used for *galca* MO and *galcb* MO, respectively, in all co-injection experiments. At variance with what observed in single *galca* or *galcb* morphants, the simultaneous injection of *galca* and *galcb* MOs resulted in a complete loss of GALC activity in double *galca/galcb* morphants that was paralleled by the disappearance of immunoreactive Galc protein in the embryo extract (Fig. 5C). In keeping with the transient nature of MO-mediated gene downregulation [20,21], RT-PCR analysis performed on zebrafish morphants at 72 hpf showed a partial recovery in the expression of mature, normally spliced *galca* and *galcb* mRNAs (data not shown). Thus, all the following experiments were performed within the first 48 h after MO injection unless described otherwise.

Constitutive GALC deficiency results in the accumulation of the toxic metabolite psychosine in GLD patients and *twitcher* mice. To assess whether the rapid *galca/galcb* down-regulation that occurs in zebrafish embryos after MO injection may exert a similar effect, we measured the levels of psychosine in the extracts of control and double *galca/galcb* morphants by mass spectrometry. The results of the analysis showed that psychosine (evaluated as galactosyl-sphingosine plus glucosyl-sphingosine) was undetectable at all the time points investigated

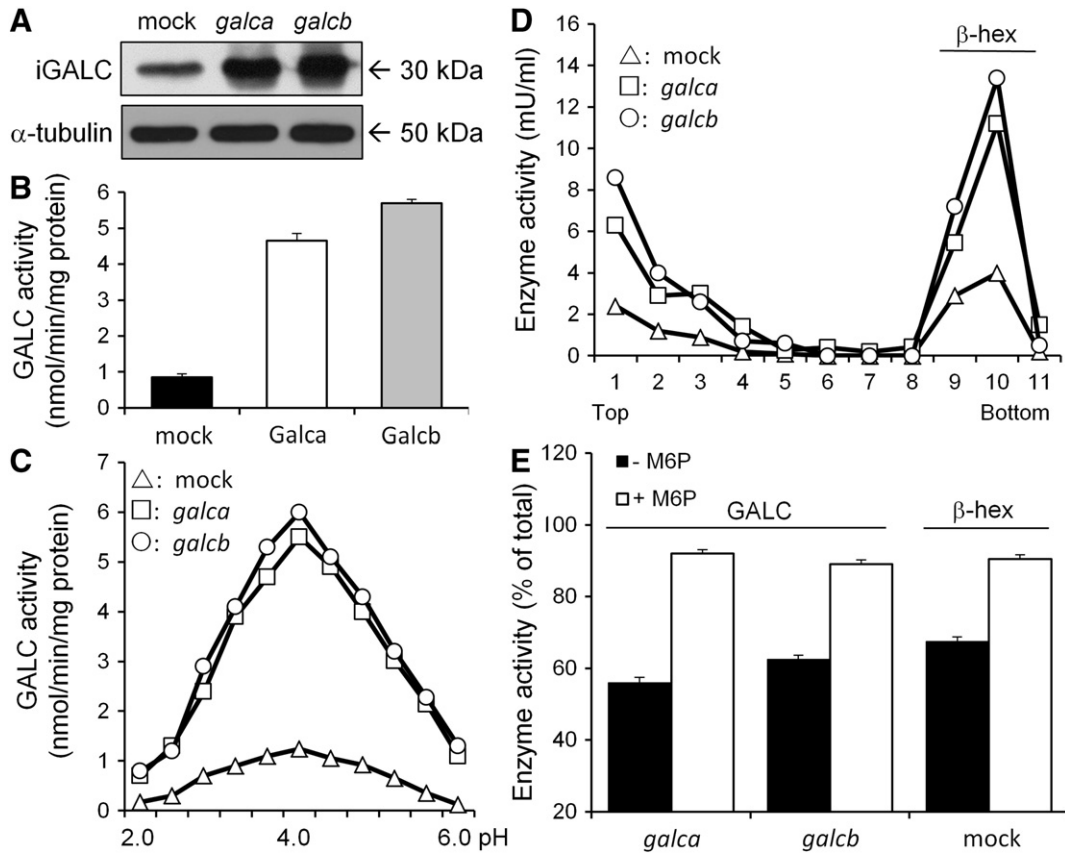


**Fig. 3.** Biochemical characterization of zebrafish Galca and Galcb enzymes in HEK 293T transfected cells. A, Total cell extracts (4.0  $\mu$ g or protein) from HEK 293T cells transfected with empty expression vector (mock) or vectors harboring the zebrafish *galca* or *galcb* cDNA were analyzed by Western blotting using a polyclonal anti-GALC antibody (iGALC);  $\alpha$ -tubulin was used for normalization. B, The same extracts were assayed for GALC activity at pH 4.0. Values are the mean  $\pm$  SD of 5 independent experiments. C, Cell extracts of mock ( $\Delta$ ), *galca* ( $\square$ ) and *galcb* ( $\circ$ ) HEK 293T transfectants were assayed for GALC activity at different pH values of incubation and results are representative of 5 independent experiments. D, Subcellular fractionation on Percoll density gradient of the cell extracts of mock ( $\Delta$ ), *galca* ( $\square$ ) and *galcb* ( $\circ$ ) HEK 293T transfectants. Both Galca and Galcb enzymatic activities co-sediment with the lysosomal  $\beta$ -hexosaminidase enzyme marker ( $\beta$ -hex). Values are representative of 3 independent experiments. E, HEK 293T transfectants were incubated in the absence (black bar) or in the presence (open bar) of 5 mM mannose-6-phosphate (M6P). After 48 h, cell extracts and conditioned media were assayed for GALC and  $\beta$ -hexosaminidase activities and released activity was calculated as percentage of total activity. Values are the mean  $\pm$  SD of 5 independent experiments.

(ranging from 24 hpf to 72 hpf), indicating that a rapid and transient GALC activity knock-down does not result in the accumulation of this metabolite in zebrafish embryos (Supplementary Fig. 5). Screening for the presence of psychosines with a long chain base other than sphingosine was also performed in zebrafish embryos, although none was present in morphant extracts (data not shown).

In keeping with the lack of major phenotypic alterations in heterozygous GLD patients and *twitcher* mice, no morphological alterations were observed in single knockdown *galca* or *galcb* zebrafish morphants in which a significant GALC activity was retained. No significant macroscopic phenotypic alterations occurred also when the complete down-regulation of GALC activity was achieved by co-injection of both splicing-inhibiting MOs in the same embryo (data not shown).

To gain insights into possible molecular alterations of CNS following the double knockdown of *galca* and *galcb* genes, we performed WISH analysis to investigate the expression pattern of various CNS markers during zebrafish development. We did not observe significant alterations of the expression of the neural marker *wnt1* [42] and of the cranial and trunk neural crest marker *crestin* [43] during somitogenesis in double *galca/galcb* morphants. Also, no significant modifications of the expression of *pax2.1*, one of the earliest genes activated during development of the midbrain and midbrain–hindbrain boundary [44], and of *emx1*, a homeobox gene early expressed in anterior brain [45], occurred in these embryos (data not shown). In contrast, a reduction and partial disorganization in the expression of the basic helix–loop–helix transcription factor *neuroD* [24] was detectable by WISH analysis of the double *galca/galcb* morphants at 24 hpf. In particular, down-regulation

of *neuroD* expression was observed in the lateral line ganglia, telencephalon and otic vesicle (20/49 embryos, data not shown). *NeuroD* expression was even more compromised when double *galca/galcb* morphants were examined at 48 hpf (Fig. 6A). Indeed, 71% of double morphants ( $n = 45$ ) showed an altered *neuroD* expression pattern versus 11% of control embryos ( $n = 66$ ). Co-injection of both splicing-inhibiting MOs caused in fact a partial or complete down-regulation of *neuroD* expression in the hindbrain and midbrain–hindbrain boundary in 22% of double *galca/galcb* morphants with an even more severe phenotype that included also *neuroD* down-regulation in the midbrain region in 49% of injected embryos (Fig. 6A). Only minor alterations of *neuroD* expression were observed in single *galca* or *galcb* morphants (data not shown), indicating that a partial reduction in GALC activity results in a phenotype similar to wild-type embryos. Of note, at variance with *neuroD* expression data, no significant changes were observed for the pattern expression of the transcription factor *neurogenin-1*, an upstream regulator of *neuroD* [46] (data not shown).

*NeuroD* is required for the survival of various subtypes of developing neurons in the vertebrate CNS [47]. On this basis, a quantitative acridine orange apoptosis test [36] was performed on double *galca/galcb* morphants. As shown in Fig. 6B, GALC activity knockdown results in a significant increase of apoptotic events, mainly localized in the head region of the embryo. This occurred in the absence of significant histological alterations and lack of globoid cells in the CNS of these embryos (data not shown). To the best of our knowledge, these data represent the first evidence of early alterations of CNS development following GALC loss-of-function.

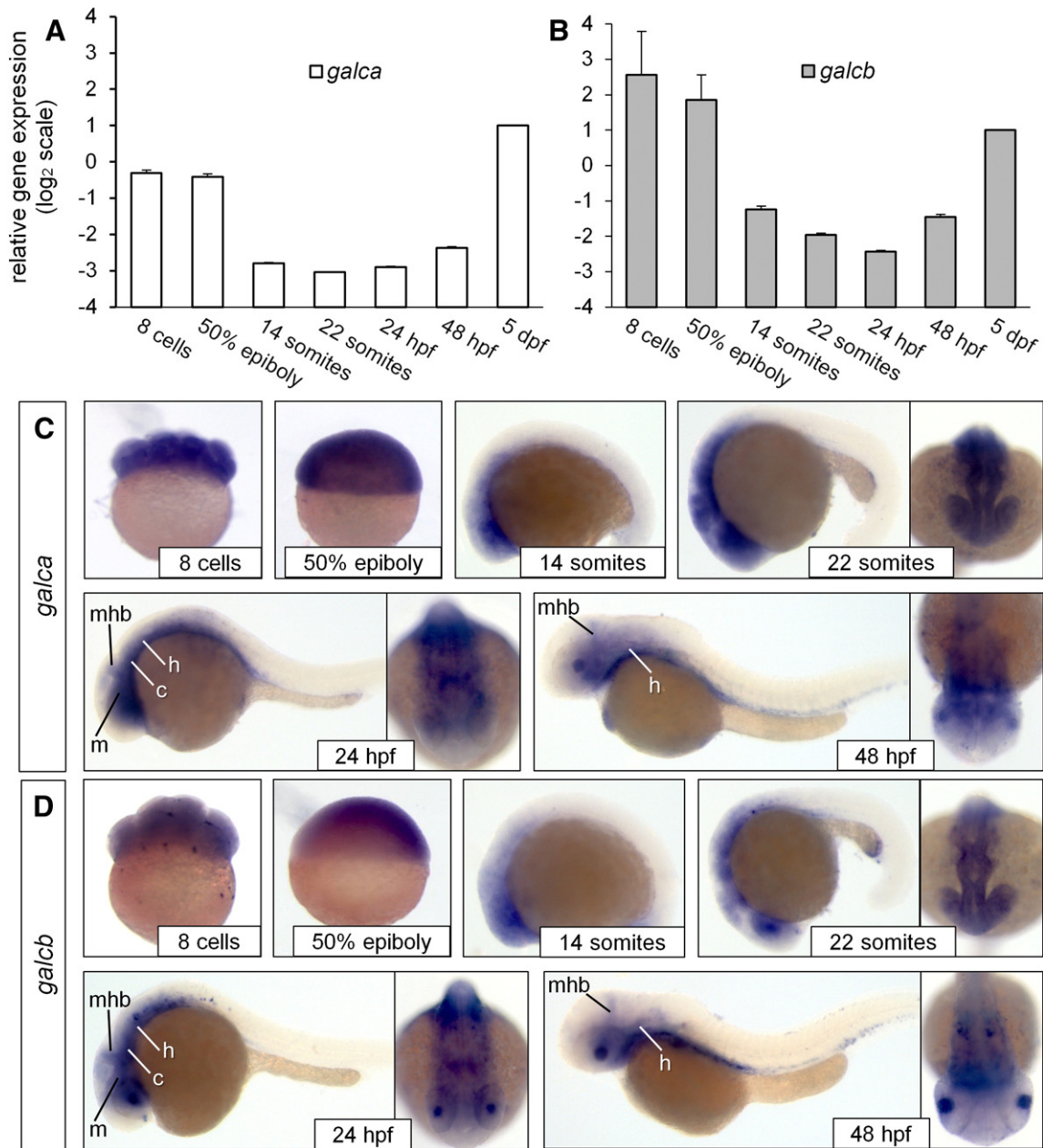


**Fig. 4.** Embryonic expression pattern of *galca* and *galcb*. A, B, Total RNA was extracted from zebrafish embryos at the indicated developmental stages and analyzed for *galca* (A) and *galcb* (B) expression by quantitative RT-PCR. Averaged data were normalized for 18S RNA expression and plotted on a log<sub>2</sub> scale. C–D, WISH analysis of the expression of *galca* (C) and *galcb* (D) genes was performed on zebrafish embryos at different stages of development. Already detectable at 1.25 hpf (8-cells stage), both genes are expressed at the animal pole at 5 hpf (50% epiboly) where CNS formation originates from ectoderm. *galca* and *galcb* transcripts are detectable in the rostral part of the embryo throughout somitogenesis. At 24 hpf, *galca* and *galcb* are co-expressed in different CNS structures including hindbrain, midbrain and cerebellum. CNS co-expression of the two genes is retained at 48 hpf. c, cerebellum; h, hindbrain; m, midbrain; mhb, midbrain–hindbrain boundary.

#### 4. Discussion

In the present work, we demonstrate the presence of GALC activity in zebrafish adults and embryos. Accordingly, *in silico* analysis identified two zebrafish genes co-ortholog to mammalian GALC named *galca* and *galcb* as indicated by their conserved synteny and exon/intron organization, high amino acid sequence identity and similar predicted protein structure. When transduced in HEK cells, both genes encode for enzymatically active proteins with lysosomal localization and a pH optimum equal to 4.0. WISH experiments demonstrated that *galca* and *galcb* are dynamically expressed in CNS during zebrafish development. Already detectable at 1.25 and 5 hpf, the expression of *galca* and *galcb* persists in developing CNS during the segmentation period whereas the signal is progressively excluded from the notochord. At 24 hpf, the expression of

both genes is observed in midbrain, midbrain–hindbrain boundary, hindbrain and cerebellum, to be maintained mainly in midbrain–hindbrain boundary and hindbrain at 48 hpf.

Similar to that observed in heterozygous GLD patients and heterozygous *twitcher* mice, no alterations occurred in single knockdown *galca* or *galcb* zebrafish morphants in which a significant GALC activity is retained. Given the apparent overlapping co-expression of *galca* and *galcb* in zebrafish CNS during development, these data suggest that the two genes may encode for proteins with similar enzymatic and biological functions and that the residual GALC activity present in the single morphants is sufficient to guarantee an apparently normal developmental process in zebrafish embryos. The simultaneous knockdown of *galca/galcb* genes resulted instead in the complete down-regulation of GALC activity in zebrafish embryos. Even though no evident phenotypic

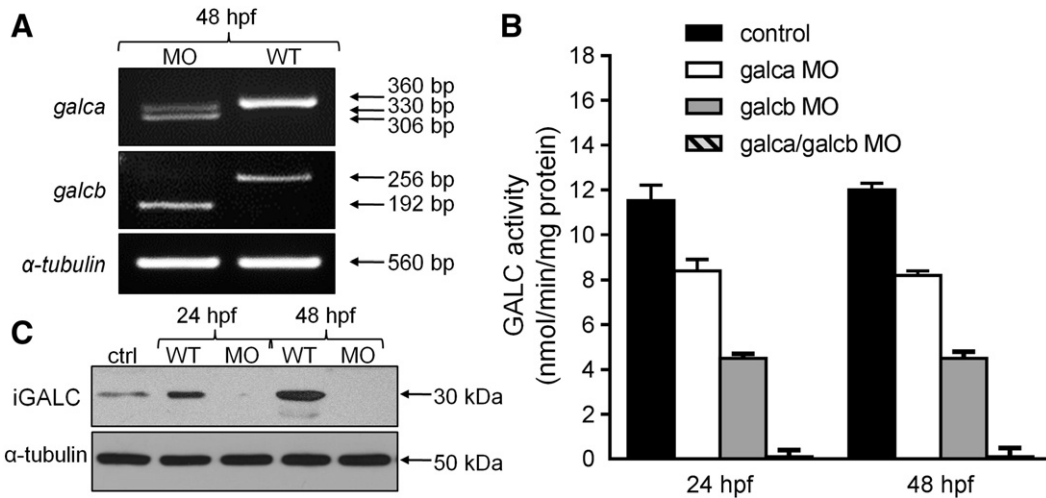


**Fig. 5.** *galca/galcb* double knockdown in zebrafish embryos. **A**, RT-PCR alternative splicing pattern analysis of 48 hpf double *galca/galcb* morphants showing the efficacy of the two exon-skipping MOs when compared to wild-type (WT) embryos.  $\alpha$ -Tubulin serves as control. **B**, Total extracts from wild-type embryos, single *galca*, single *galcb* and double *galca/galcb* morphants were assayed for GALC activity. Negligible activity was detectable in double *galca/galcb* morphants. The results are the mean  $\pm$  SD of 3 independent experiments. **C**, No GALC immunoreactive proteins (iGALC) were found when the extracts of double *galca/galcb* morphants (MO) were analyzed by Western blotting using a polyclonal anti-GALC antibody.  $\alpha$ -Tubulin was used for normalization. ctrl: control murine brain extract.

alterations were observed in double morphants, *galca/galcb* knockdown caused a significant reduction and partial disorganization in the expression of the basic helix–loop–helix transcription factor *neuroD* [24] during CNS development. Alterations of the expression of this neural marker

occurred in CNS regions of zebrafish embryo in which both *galca* and *galcb* are highly expressed, including midbrain, midbrain–hindbrain boundary and hindbrain. At variance, only minor modifications, if any, were observed in these embryos for the neural marker *wnt1* [42], the

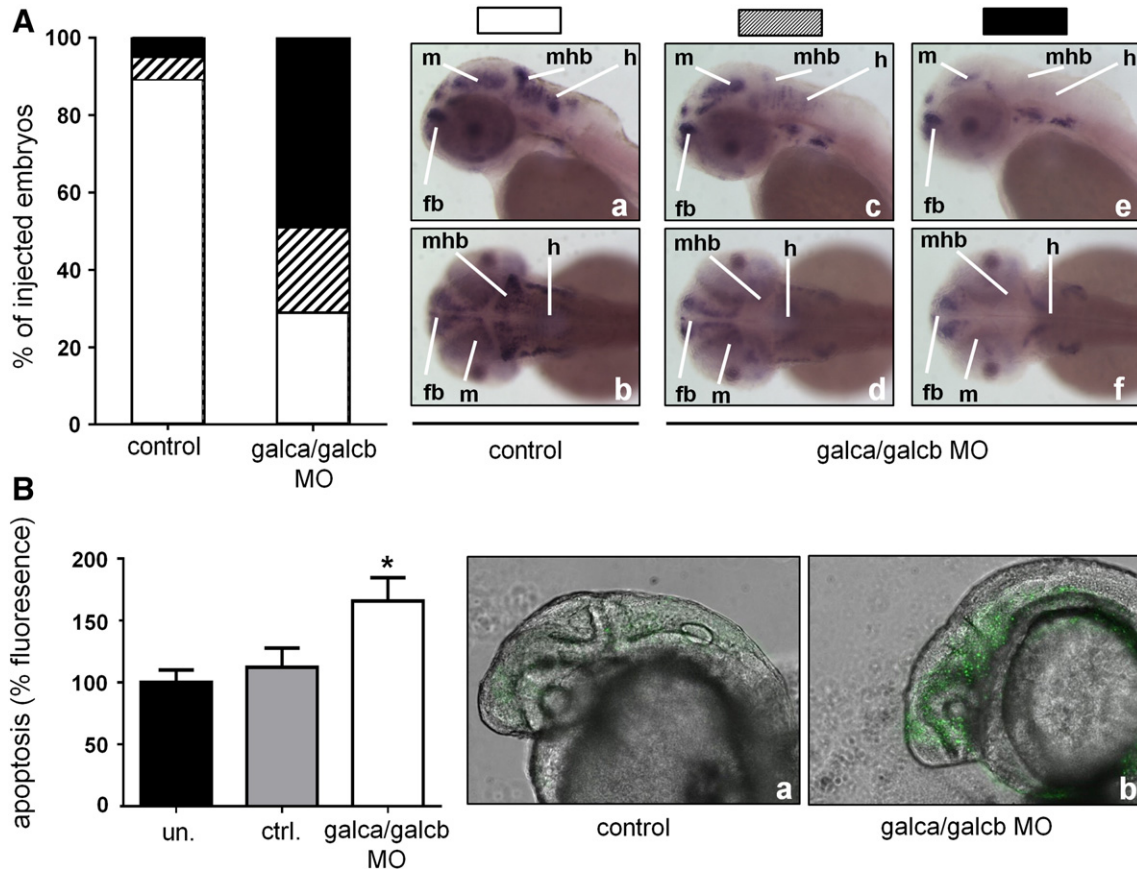


**Fig. 6.** *galca/galcb* double knockdown affects *neuroD* expression and apoptosis in zebrafish embryos. **A**, The expression of the neural marker *neuroD* was analyzed by WISH in control ( $n = 66$ ) and double *galca/galcb* morphants ( $n = 45$ ) at 48 hpf. *NeuroD* expression was scored as normal (open bar and panels a, b), down-regulated in midbrain–hindbrain boundary and hindbrain (dashed bar and panels c, d), and down-regulated in midbrain–hindbrain boundary, midbrain and hindbrain (black bar and panels e, f). Lateral and top view of representative control embryos (a, b) and of double *galca/galcb* morphants (c–f). fb, forebrain; h, hindbrain; mhb, midbrain–hindbrain boundary; m, midbrain. **B**, Untreated (un.), control (ctrl.) and double *galca/galcb* morphants were assessed at 24 hpf for apoptotic events by acridine orange staining followed by measurement of total fluorescence in embryo extracts ( $n = 30$ ). Representative images of the head region of acridine orange-stained control (a) and double *galca/galcb* morphant (b) embryos. \*,  $P < 0.05$ , Student's *t* test.

cranial and trunk neural crest marker *crestin* [43], the midbrain and midbrain–hindbrain boundary gene *pax2.1* [44], the early anterior brain homeobox gene *emx1* [45], and the upstream *neuroD* regulator *neurogenin-1* [46]. This indicates that the selective down-regulation of *neuroD* expression observed during CNS development does not represent the mere consequence of non-specific neurotoxic effects consequent to *galca/galcb* loss-of-function. Even though further experiments are required to investigate the role of GALC in the modulation of *neuroD* expression, our data indicate that the complete down-regulation of GALC activity in double *galca/galcb* morphants may result in significant changes of CNS development in zebrafish. Indeed, we observed an increase of apoptotic events in the head region of double *galca/galcb* morphants, in keeping with the premature neuronal death that occurs at early stages of neurogenesis in *NeuroD* null mice [47].

Lysosomal storage disorders are characterized by the accumulation of disease-specific metabolic intermediates [2]. The pathogenesis of GLD has been proposed to arise from the accumulation of psychosine, the neurotoxic lysolipid metabolite detected at high levels in the CNS of GLD patients [2–4]. Accumulation of psychosine leads to cytotoxic effects on oligodendroglial cells and progressive demyelination, triggering apoptotic cell death [48–50] and resulting in a severe neurological dysfunction [5–7]. However, no psychosine was detectable by mass spectrometry analysis of the embryo extracts of double *galca/galcb* morphants at all the time points investigated. Likely, the limited period of *galca/galcb* knockdown dictated by the transient inhibitory effect exerted by MOs [20,21] did not allow a significant accumulation of psychosine in zebrafish embryos. Relevant to this point, oligodendrocyte-driven CNS myelination in zebrafish starts in the hindbrain at day 4 of development and it is not yet completed at day 10 [51], making the study of the effect of GALC activity knockdown on myelination in zebrafish morphants unfeasible.

Even though the above limitations indicate that double *galca/galcb* zebrafish morphants do not represent a model of advanced human GLD, the observed alterations of *neuroD* expression in these embryos, paralleled by an increase of apoptotic events, indicate that GALC loss-of-function may have early pathological consequences independent of psychosine accumulation, thus providing novel insights into the pathogenesis of GLD. This possibility is supported by a recent study about the impact of a spontaneous missense *Galc* mutation in *twi-5J* mice in which psychosine levels do not correlate with nervous system regions exhibiting demyelination and axonopathy [52]. Thus, double *galca/galcb* zebrafish morphants represent an attractive option for addressing previously unrecognized psychosine-independent key aspects of the pathogenesis of GLD. Further studies will be required to assess the impact of *galca/galcb* down-regulation on the sphingolipid profile in zebrafish embryos and to elucidate the molecular mechanism(s) responsible for the observed alterations in *neuroD* expression that follow the loss of GALC activity.

Given the limited progresses toward an efficacious clinical treatment of GLD patients [7,8], novel model systems may provide an invaluable tool for investigating the molecular mechanisms underlying GLD in the search for effective therapeutic interventions. At present, murine models of GLD are widely used to understand the molecular and biochemical bases of the disease and for the search of novel therapeutic approaches [9–12,52]. Nevertheless, such studies in mice can be relatively slow, laborious and expensive to perform. Also, the intrauterine gestation makes it difficult to follow possible alterations in early developmental processes as a consequence of the lack of GALC activity. To this respect, zebrafish have significant advantages over mice in producing hundreds of externally fertilized eggs that develop *in vitro* as optically transparent embryos, allowing live manipulations and observations from the earliest stages of development. Our findings underscore the potentiality of the zebrafish system in studying the pathogenesis of lysosomal neurodegenerative diseases, including GLD. The lack of lethal embryonic defects in zebrafish *galca/galcb* morphants pave the way for generating stable *galca/galcb* single and double gene knock-out

zebrafish lines by TALEN or CRISPR/Cas targeting technology [22,23]. These zebrafish lines will provide further insights for the development of novel GLD animal models and for the search of efficacious therapeutic strategies.

Supplementary data to this article can be found online at <http://dx.doi.org/10.1016/j.bbdis.2014.01.008>.

## Acknowledgements

This work was supported in part by grants from Ministero dell'Istruzione, Università e Ricerca (MIUR, Centro IDET, FIRB project RBAP11H2R9 2011) and Associazione Italiana per la Ricerca sul Cancro (AIRC grant no. 10396) to MP. EDS was supported by a fellowship from Fondazione Umberto Veronesi, Italy. The authors wish to thank F. Cotelli (University of Milan) for helpful advice and criticisms, R. Giuliani for help in GALC activity assays, E. Dalmau for UPLC/TOF analyses and S. Mitola for help in apoptosis assay.

## References

- [1] K. Suzuki, Y. Suzuki, Globoid cell leucodystrophy (Krabbe's disease): deficiency of galactocerebroside beta-galactosidase, Proc. Natl. Acad. Sci. U. S. A. 66 (1970) 302–309.
- [2] A. Ballabio, V. Gieselmann, Lysosomal disorders: from storage to cellular damage, Biochim. Biophys. Acta 1793 (2009) 684–696.
- [3] K. Suzuki, Twenty five years of the "psychosine hypothesis": a personal perspective of its history and present status, Neurochem. Res. 23 (1998) 251–259.
- [4] H. Igisu, K. Suzuki, Progressive accumulation of toxic metabolite in a genetic leukodystrophy, Science 224 (1984) 753–755.
- [5] K. Suzuki, Globoid cell leukodystrophy (Krabbe's disease): update, J. Child Neurol. 18 (2003) 595–603.
- [6] M.C. Loonen, O.P. Van Diggelen, H.C. Janse, W.J. Kleijer, W.F. Arts, Late-onset globoid cell leucodystrophy (Krabbe's disease). Clinical and genetic delineation of two forms and their relation to the early-infantile form, Neuroepidemiology 16 (1985) 137–142.
- [7] D.A. Wenger, M.A. Rafi, P. Luzzi, J. Datto, E. Costantino-Ceccarini, Krabbe disease: genetic aspects and progress toward therapy, Mol. Genet. Metab. 70 (2000) 1–9.
- [8] N. Sakai, Pathogenesis of leukodystrophy for Krabbe disease: molecular mechanism and clinical treatment, Brain Dev. 31 (2009) 485–487.
- [9] K. Suzuki, The twitcher mouse: a model for Krabbe disease and for experimental therapies, Brain Pathol. 5 (1995) 249–258.
- [10] A. Lattanzi, M. Neri, C. Maderna, I. di Girolamo, S. Martino, A. Orlacchio, M. Amendola, L. Naldini, A. Gritti, Widespread enzymatic correction of CNS tissues by a single intracerebral injection of therapeutic lentiviral vector in leukodystrophy mouse models, Hum. Mol. Genet. 19 (2010) 2208–2227.
- [11] M. Strazza, A. Luddi, M. Carbone, M.A. Rafi, E. Costantino-Ceccarini, D.A. Wenger, Significant correction of pathology in brains of twitcher mice following injection of genetically modified mouse neural progenitor cells, Mol. Genet. Metab. 97 (2009) 27–34.
- [12] F. Galbiati, M.I. Givogri, L. Cantuti, A.L. Rosas, H. Cao, R. van Breemen, E.R. Bongarzone, Combined hematopoietic and lentiviral gene-transfer therapies in newborn twitcher mice reveal contemporaneous neurodegeneration and demyelination in Krabbe disease, J. Neurosci. Res. 87 (2009) 1748–1759.
- [13] B.A. Barut, L.J. Zon, Realizing the potential of zebrafish as a model for human disease, Physiol. Genomics 2 (2000) 49–51.
- [14] A. Dodd, P.M. Curtis, L.C. Williams, D.R. Love, Zebrafish: bridging the gap between development and disease, Hum. Mol. Genet. 9 (2000) 2443–2449.
- [15] L.A. Lowery, H. Sive, Strategies of vertebrate neurulation and a re-evaluation of teleost neural tube formation, Mech. Dev. 121 (2004) 1189–1197.
- [16] J.J. Sager, Q. Bai, E.A. Burton, Transgenic zebrafish models of neurodegenerative diseases, Brain Struct. Funct. 214 (2010) 285–302.
- [17] H. Flanagan-Steet, C. Sias, R. Steet, Altered chondrocyte differentiation and extracellular matrix homeostasis in a zebrafish model for mucopolysaccharidosis II, Am. J. Pathol. 175 (2009) 2063–2075.
- [18] O. Bandmann, E.A. Burton, Genetic zebrafish models of neurodegenerative diseases, Neurobiol. Dis. 40 (2010) 58–65.
- [19] Y. Xi, S. Noble, M. Ekker, Modeling neurodegeneration in zebrafish, Curr. Neurol. Neurosci. Rep. 11 (2011) 274–282.
- [20] A. Nasevicius, S.C. Ekker, Effective targeted gene 'knockdown' in zebrafish, Nat. Genet. 26 (2000) 216–220.
- [21] V.M. Bedell, S.E. Westcot, S.C. Ekker, Lessons from morpholino-based screening in zebrafish, Brief. Funct. Genomics 10 (2011) 181–188.
- [22] P. Huang, Z. Zhu, S. Lin, B. Zhang, Reverse genetic approaches in zebrafish, J. Genet. Genomics 39 (2012) 421–433.
- [23] W.Y. Hwang, Y. Fu, D. Reyon, M.L. Maeder, S.Q. Tsai, J.D. Sander, R.T. Peterson, J.R. Yeh, J.K. Joung, Efficient genome editing in zebrafish using a CRISPR–Cas system, Nat. Biotechnol. 31 (2013) 227–229.
- [24] T. Mueller, M.F. Wullmann, Expression domains of *neuroD* (*nrd*) in the early postembryonic zebrafish brain, Brain Res. Bull. 57 (2002) 377–379.
- [25] M. Westerfield, The Zebrafish Book, University of Oregon Press, Eugene, OR, 1995.
- [26] C.B. Kimmel, W.W. Ballard, S.R. Kimmel, B. Ullmann, T.F. Schilling, Stages of embryonic development of the zebrafish, Dev. Dyn. 203 (1995) 253–310.

- [27] S.F. Altschul, W. Gish, W. Miller, E.W. Myers, D.J. Lipman, Basic local alignment search tool, *J. Mol. Biol.* 215 (1990) 403–410.
- [28] J.D. Thompson, D.G. Higgins, T.J. Gibson, CLUSTAL W: improving the sensitivity of progressive multiple sequence alignment through sequence weighting, position-specific gap penalties and weight matrix choice, *Nucleic Acids Res.* 22 (1994) 4673–4680.
- [29] M. Muffato, A. Louis, C.E. Poisnel, H. Roest Crolius, Genomicus: a database and a browser to study gene synteny in modern and ancestral genomes, *Bioinformatics* 26 (2010) 1119–1121.
- [30] S. Martino, R. Tiribuzi, A. Tortori, D. Conti, I. Visigalli, A. Lattanzi, A. Biffi, A. Gritti, A. Orlacchio, Specific determination of beta-galactocerebrosidase activity via competitive inhibition of beta-galactosidase, *Clin. Chem.* 55 (2009) 541–548.
- [31] S. Marchesini, A. Preti, M.F. Aleo, A. Casella, A. Dagan, S. Gatt, Synthesis, spectral properties and enzymatic hydrolysis of fluorescent derivatives of cerebroside sulfate containing long-wavelength-emission probes, *Chem. Phys. Lipids* 53 (1990) 165–175.
- [32] R. Bresciani, K. von Figura, Dephosphorylation of the mannose-6-phosphate recognition marker is localized in later compartments of the endocytic route. Identification of purple acid phosphatase (uteroferrin) as the candidate phosphatase, *Eur. J. Biochem.* 238 (1996) 669–674.
- [33] A.T. McCurley, G.V. Callard, Characterization of housekeeping genes in zebrafish: male–female differences and effects of tissue type, developmental stage and chemical treatment, *BMC Mol. Biol.* 9 (2008) 102.
- [34] M.W. Pfaffl, G.W. Horgan, L. Dempfle, Relative expression software tool (REST) for group-wise comparison and statistical analysis of relative expression results in real-time PCR, *Nucleic Acids Res.* 30 (2002) e36.
- [35] C. Thisse, B. Thisse, High-resolution in situ hybridization to whole-mount zebrafish embryos, *Nat. Protoc.* 3 (2008) 59–69.
- [36] H.W.I. Detrich, M. Westerfield, L.I. Zon, *The Zebrafish: Cellular and Developmental Biology*, 2nd ed. Elsevier Academic Press, 2004.
- [37] D. Canals, D. Mormeneo, G. Fabrias, A. Llebaria, J. Casas, A. Delgado, Synthesis and biological properties of Pachastrissamine (jaspine B) and diastereoisomeric jaspines, *Bioorg. Med. Chem.* 17 (2009) 235–241.
- [38] J.E. Deane, S.C. Graham, N.N. Kim, P.E. Stein, R. McNair, M.B. Cachon-Gonzalez, T.M. Cox, R.J. Read, Insights into Krabbe disease from structures of galactocerebrosidase, *Proc. Natl. Acad. Sci. U. S. A.* 108 (2011) 15169–15173.
- [39] B.L. Cantarel, P.M. Coutinho, C. Rancurel, T. Bernard, V. Lombard, B. Henrissat, The Carbohydrate-Active EnZymes database (CAZy): an expert resource for Glycogenomics, *Nucleic Acids Res.* 37 (2009) D233–D238.
- [40] J.H. Postlethwait, I.G. Woods, P. Ngo-Hazlett, Y.L. Yan, P.D. Kelly, F. Chu, H. Huang, A. Hill-Force, W.S. Talbot, Zebrafish comparative genomics and the origins of vertebrate chromosomes, *Genome Res.* 10 (2000) 1890–1902.
- [41] K. Kollmann, S. Pohl, K. Marschner, M. Encarnacao, I. Sakwa, S. Tiede, B.J. Poorthuis, T. Lubke, S. Muller-Loennies, S. Storch, T. Brailke, Mannose phosphorylation in health and disease, *Eur. J. Cell Biol.* 89 (2009) 117–123.
- [42] A.C. Lekven, G.R. Buckles, N. Kostakis, R.T. Moon, Wnt1 and wnt10b function redundantly at the zebrafish midbrain–hindbrain boundary, *Dev. Biol.* 254 (2003) 172–187.
- [43] R. Luo, M. An, B.L. Arduini, P.D. Henion, Specific pan-neural crest expression of zebrafish Crestin throughout embryonic development, *Dev. Dyn.* 220 (2001) 169–174.
- [44] A. Picker, S. Scholpp, H. Bohli, H. Takeda, M. Brand, A novel positive transcriptional feedback loop in midbrain–hindbrain boundary development is revealed through analysis of the zebrafish pax2.1 promoter in transgenic lines, *Development* 129 (2002) 3227–3239.
- [45] K.H. Krabbe, A new familial infantile form of diffuse brain-sclerosis, *Brain* 39 (1916) 74–115.
- [46] V. Korzh, I. Sleptsova, J. Liao, J. He, Z. Gong, Expression of zebrafish bHLH genes *ngn1* and *nrd* defines distinct stages of neural differentiation, *Dev. Dyn.* 213 (1998) 92–104.
- [47] W.Y. Kim, NeuroD regulates neuronal migration, *Mol. Cells* 35 (2013) 444–449.
- [48] M. Jatana, S. Giri, A.K. Singh, Apoptotic positive cells in Krabbe brain and induction of apoptosis in rat C6 glial cells by psychosine, *Neurosci. Lett.* 330 (2002) 183–187.
- [49] M. Zaka, D.A. Wenger, Psychosine-induced apoptosis in a mouse oligodendrocyte progenitor cell line is mediated by caspase activation, *Neurosci. Lett.* 358 (2004) 205–209.
- [50] E. Haq, S. Giri, I. Singh, A.K. Singh, Molecular mechanism of psychosine-induced cell death in human oligodendrocyte cell line, *J. Neurochem.* 86 (2003) 1428–1440.
- [51] C. Brosamle, M.E. Halpern, Characterization of myelination in the developing zebrafish, *Glia* 39 (2002) 47–57.
- [52] G.B. Potter, M. Santos, M.T. Davison, D.H. Rowitch, D.L. Marks, E.R. Bongarzone, M.A. Petryniak, Missense mutation in mouse GALC mimics human gene defect and offers new insights into Krabbe disease, *Hum. Mol. Genet.* 22 (2013) 3397–3414.